Hindawi
Mathematical Problems in Engineering
Volume 2021, Article ID 6624893, 18 pages
https://doi.org/10.1155/2021/6624893

Research Article

Composite Curve Path following an Underactuated AUV

Ben Li,[1] **Guohua Xu**,[1,2] **Yingkai Xia**,[3] **Wenjin Wang**,[1] **and Zhen Su**[1]

[1]*School of Naval Architecture and Ocean Engineering, Huazhong University of Science and Technology, Wuhan 430074, China*
[2]*Hubei Key Laboratory of Naval Architecture and Ocean Engineering Hydrodynamics, HUST, Wuhan 430074, China*
[3]*College of Engineering, Huazhong Agricultural University, Wuhan 430070, China*

Correspondence should be addressed to Guohua Xu; hustxu@vip.sina.com and Yingkai Xia; ykxia@mail.hzau.edu.cn

Received 16 December 2020; Revised 23 February 2021; Accepted 25 March 2021; Published 8 April 2021

Academic Editor: Chih-Chiang Chen

This paper addresses the problem of composite curve path following for an underactuated autonomous underwater vehicle by utilizing an adaptive integral line-of-sight (AILOS) guidance and nonlinear iterative sliding mode (NISM) controller. First, the composite curve path is parametrized by a common scalar variable in a continuous way. Then, the kinematics error of an underactuated vehicle is described based on the nonprojection Frenet–Serret frame with a virtual point, which can be eliminated by the virtual point control and AILOS guidance. Meanwhile, the subpath switching algorithm is studied to realize the global path following for the composite curve path. Besides, the NISM controller is cascaded with the AILOS guidance law, and the cascade structure proved to be globally κ-exponentially stable under the influence of slow time-varying currents. Finally, simulations are considered to demonstrate the effectiveness of the proposed composite curve path following control scheme.

1. Introduction

In recent years, much research has been done in the field of path following for autonomous underwater vehicles (AUVs). In most of the existing literature, the desired geometric path is a single curve [1, 2]. However, as is known, a single curve cannot represent complex shapes with a high degree; it may result in a very intractable and impractical path due to Runge's phenomenon [3]. Hence, utilizing the composite curve path as the desired path is more practical since it is composed of multiple subpaths and can meet the demands of varied tasks flexibly in a complex and limited marine environment.

It is known that the shape and the properties of the composite curve path have a great influence on the path following control. Generally, the composite curve path is obtained by a path planning algorithm with two steps. Firstly, utilizing a path search algorithm, the given order of waypoints is obtained based on certain optimization objectives. Then, considering the kinematics constraints of the vehicle, multiple curves (such as straight lines, circular arcs, spiral lines, and polynomial curves) can be used to connect all the waypoints to generate a flyable path [4]. In the existing literature, path following of composite curve path such as successive straight lines, straight lines and circles [5,6], and spline interpolation curve [7] has been studied. However, to the best of the authors' knowledge, no general method has been proposed for tracking the composite curve path, which will be studied in this paper.

As the expressions of curve segments vary, and there is no unified parametrization for the composite curve path, they will be inconvenient to calculate and expand. Hence, for better tracking of the composite curve path, it is necessary to choose an appropriate path description method. To solve this problem, all the curve segments are parametrized in a continuous way in this paper. Besides, each curve segment is parametrized by a common scalar variable with the same interval. However, it is usually difficult for the composite curve path to satisfy parametric continuity between the curve segments. Hence, to realize the global path following of the composite curve path, the problem of subpath switching [5, 8] is also discussed.

After the composite curve path has been designed and parametrized, an efficient path following system is proposed. For underactuated AUVs, which have no independent control input in the sway and heaven direction, the line-of-sight (LOS) guidance principle is a very suitable and efficient

solution for path following. When combined with guidance, the position and heading can be controlled simultaneously just by the heading control. Hence, utilizing LOS guidance, this has been no longer an underactuated problem in terms of the variables to be controlled [9]. Proportional LOS guidance is one of the most widely used methods [10]. However, it cannot handle the unknown environmental disturbance such as wind, wave, or currents. To solve this problem, the integral line-of-sight (ILOS) guidance law is proposed for path following of straight-line paths in the presence of constant and irrotational ocean currents [11]. A modified version of the ILOS algorithm based on the adaptive compensation of the sideslip angle is proposed for path following of a parametrized curve under unknown environmental disturbances [6]. Besides, adaptive integral line-of-sight (AILOS) guidance law is designed for marine craft exposed to ocean currents. The expression of the cross-track kinematics error is reformulated using the concept of relative velocity [12].

Generally, the LOS guidance laws are intuitive as they are formulated at a kinematics level without using the vehicle parameters. Through a cascaded system approach [13], the LOS guidance principle can be interconnected with a heading controller to achieve the path following control. In detail, the LOS guidance principle transforms the position error into the desired heading angle, and the heading control system is responsible for eliminating the heading error. For the cascaded system, the heading controller can be designed independently, so more concise control law can be obtained, such as the PID (proportional integral derivative) control, the fuzzy control, the sliding mode control, and the neural network control. Different control algorithms have their own advantages and disadvantages. In [6], to realize the LOS path following for Dubins paths, the PID controller has been used for the heading control, which is easy to implement, but there are the problems of integral saturation and slow convergence speed. Sliding mode control has strong robustness against external environmental disturbances. In [12], the sliding mode control is constructed for the heading control. However, the control law is based on the yaw dynamics model and can be affected by the uncertainty of model parameters. In [14], disturbance observers and modified terminal sliding mode control are combined to design a robust disturbance rejection control law for the dynamics control of a X-rudder AUV. Fuzzy control [1] and neural network control [7,15] are usually combined with other control methods in order to identify the dynamical uncertainty and time-varying ocean disturbances.

In this paper, a new composite curve path following controller is proposed for an underactuated AUV, based on nonlinear iterative sliding mode (NISM) controller [16] and AILOS guidance. The main contributions are summarized as follows:

(1) To eliminate the tracking error, a cascade structure is established based on AILOS guidance law and a NISM controller, which proved to be UGAS (uniformly globally asymptotically stable).

(2) Based on the AILOS guidance law and the subpath switching algorithm, the global path following of the composite curve path in the kinematics layer is realized with the unknown ocean currents.

(3) The NISM control is proposed in the dynamics layer, which has the characteristics of fast convergence and strong antidisturbance ability. In addition, the strictly bounded nonlinear hyperbolic tangent function is used to avoid excessive control input caused by the discontinuity at each connection point between two subpaths. Besides, the incremental feedback control law is designed, which is independent of hydrodynamic parameters.

The remainder of this paper is organized as follows. Section 2 describes the concept and parametrization of the composite curve path, where the continuity characteristics of the composite curve path are analyzed, and parametric forms of common curves are given. Section 3 presents the kinematics and dynamics expressions of REMUS (remote environmental monitoring units) vehicles and problem formulation. Section 4 addresses the design and proof of the path following control system. Section 5 validates the effectiveness of the previous design for the composite curve path following with several simulation cases and discussions. Section 6 demonstrates the conclusion of this work.

2. Preliminaries

The composite curve path can be defined as a set of curves connected in a specific order. Each curve segment is regarded as a subpath. The parametrization and the continuity of the composite curve path are discussed in this section. Besides, the parametric description is proposed for typical curves.

2.1. Path Parametrization. In complex and limited marine environment, the composite paths can meet the demands of varied tasks flexibly by adjusting the type of subpaths. However, as the expressions of subpaths may vary, they will be inconvenient to calculate and hard to expand for the path following of composite curve path.

To handle this problem, the path parametrization method is adopted to describe the composite curve path. Many parametrization methods can be used to describe a path, which may be continuous, discrete, or even hybrid [17]. In this paper, the composite curve path is parametrized in a continuous way, and every curve segment is parametrized by a common scalar variable $s \in [0, n]$ (n is a natural number) with the same interval, which makes it more convenient to calculate considering different kinds of curve segments.

For a continuous parametrization, the composite curve path L with n subpaths can be defined as

$$p_p(s) \coloneqq \begin{cases} L_1(s), & s \in [0,1), \\ L_2(s), & s \in [1,2), \\ \vdots & \\ L_i(s), & s \in [i-1,i), \\ \vdots & \\ L_n(s), & s \in [n-1,n]. \end{cases} \tag{1}$$

The path is then simplified by the set

$$L \coloneqq \left\{ p \in \mathbb{R}^2 \colon \exists s \in [0, n] \text{ s.t. } p = p_p(s) \right\}, \tag{2}$$

where $L_i(s)$ denotes the parametrization of the i th subpath of the composite path L, and p is the set of all the points on L. The coordinates of the point $p_p(s)$ in the inertial frame $\{I\}$ are uniquely determined by a specific value $s \in [0, n]$ with the following form:

$$p_p(s) = \begin{bmatrix} x_p(s) \\ y_p(s) \end{bmatrix}. \tag{3}$$

With a continuous parametrization, for any given parameters of the composite curve path, the position of the corresponding point can be determined uniquely.

Regular curves are desired for the subpaths, which means that such paths never degenerate into a point nor do they have corners. Specifically, these curves include both straight lines and circles [18]. Parametrization for the regular curves satisfies

$$\left| p_p'(s) \right| \triangleq \left| \frac{\mathrm{d} p_p(s)}{\mathrm{d}s} \right|, \tag{4}$$

where $p_p'(s)$ is the first derivative of the point $p_p(s)$ w.r.t. the path parameter$s$. For each subpath, the first and second derivatives w.r.t. s can be described as

$$\begin{cases} x_p'(s) = \dfrac{\mathrm{d}x_p}{\mathrm{d}s} \\ y_p'(s) = \dfrac{\mathrm{d}y_p}{\mathrm{d}s}, \\ x_p''(s) = \dfrac{\mathrm{d}^2 x_p}{\mathrm{d}s^2}, \\ y_p''(s) = \dfrac{\mathrm{d}^2 y_p}{\mathrm{d}s^2}. \end{cases} \tag{5}$$

The first derivative of s w.r.t. time is $\dot{s} = (\mathrm{d}s/\mathrm{d}t)$, and the path-tangential speed is calculated as

$$U_P = \sqrt{\dot{x}_p(s)^2 + \dot{y}_p(s)^2} = \sqrt{x_p'(s)^2 + y_p'(s)^2}\,\dot{s}. \tag{6}$$

The path-tangential angle (or course angle of the path) is computed as

$$\chi_p(s) = a \tan 2 \left(\frac{y_p'(s)}{x_p'(s)} \right). \tag{7}$$

The curvature of the path can be calculated as

$$\kappa = \frac{x_p'(s) y_p''(s) - y_p'(s) x_p''(s)}{\sqrt[3]{x_p'^2(s) + y_p'^2(s)}}. \tag{8}$$

The angular speed of the path can be described as

$$r_p(s) = \dot{\chi}_p(s) = \frac{\partial \chi_p}{\partial s}\dot{s} = \frac{x_p'(s) y_p''(s) - y_p'(s) x_p''(s)}{x_p'^2(s) + y_p'^2(s)}\dot{s}. \tag{9}$$

2.2. Path Smoothness. The smoothness of the desired path has an essential impact on the motion control of the underactuated vehicle. Moreover, two notions can be used to describe the path smoothness, namely, the geometric continuity (GC) and the parametric continuity (PC) [19].

GC is denoted by G^n, with n specifying the degree of smoothness. The brief definition of GC up to the second degree can be given as follows:

(i) G^0: the only requirement is that all subpaths are connected

(ii) G^1: the path-tangential angle in the connection point is continuous

(iii) G^2: the tangential angle and the curvature of the path are continuous

Similarly, PC is denoted by C^n, with n specifying the degree of smoothness. C^n up to the second degree can be defined as follows:

(i) C^0: the definition is the same as that of G^0

(ii) C^1: the velocity vector orientation and magnitude are continuous

(iii) C^2: the acceleration is continuous

Compared with GC, PC is a stricter form of continuity which imposes constraints on how the parameter propagates along the path. Moreover, PC is a measure of smoothness for parametrizations.

From (1), it can be concluded that the composite curve path can satisfy at least the C^0 (or G^0) continuity. However, higher-order PC is usually hard to realize for the composite curve path with different types of curve segments. The derivative of the parameter in the connection point is discontinuous. Relatively, G^1 and G^2 are easy to build and can be used for path following of the composite curve path.

Some common composite curve paths can be used as examples (see Table 1).

2.3. Parametric Description of Typical Curves. Based on [19], the parametric descriptions of straight lines, circular arcs, and Fermat's spiral with a standard scalar variable are given. The parametric description of the line segment is as follows:

$$P_{\text{line}}(s) = \begin{bmatrix} x_0 + Ls\cos(\chi_l) \\ y_0 + Ls\sin(\chi_l) \end{bmatrix}, \tag{10}$$

where (x_0, y_0) is the starting point, L is the length of the line segment, and χ_l is the path-tangential angle of the line segment.

Furthermore, the parametrization of circular arcs can be expressed as

Table 1: Common composite curve paths.

Path	GC	Comments
Piecewise linear path	G^0	Generated directly through waypoints but is not suitable for path following of underactuated AUV
Circular smoothing	G^1	Generated by approximating methods, and curvature between straight and circular segments is discontinuous
Dubins path	G^1	Generated by interpolating methods, and curvature between straight and circular segments is discontinuous
Clothoid smoothing	G^2	Generated by approximating methods, linear varying curvature with an increased computational cost
Fermat's spiral smoothing	G^2	Generated by interpolating methods, curvature-continuous paths with a very low computational cost compared to clothoid smoothing [19]

$$P_{\text{cir}}(s) = \begin{bmatrix} c_{x0} + R\cos(\alpha_0 + s(\alpha_1 - \alpha_0)) \\ c_{y0} + R\sin(\alpha_0 + s(\alpha_1 - \alpha_0)) \end{bmatrix}. \tag{11}$$

Here, (c_{x0}, c_{y0}) is the center of the circle, and R is the radius. Besides, α_0 and α_1 are the heading angles of vectors from the center of the circle to the starting point and the endpoint.

To avoid singularity, the parametrization of Fermat's spiral can be described as

$$P_{\text{FS}}(s) = \begin{bmatrix} x_0 + k\sqrt{\theta_{\text{end}}}\, s\cos\left(\rho\theta_{\text{end}}s^2 + \chi_0\right) \\ y_0 + k\sqrt{\theta_{\text{end}}}\, s\sin\left(\rho\theta_{\text{end}}s^2 + \chi_0\right) \end{bmatrix}, \tag{12}$$

$$s \coloneqq \frac{\sqrt{\theta}}{\sqrt{\theta_{\text{end}}}} \Rightarrow 0 \le s \le 1.$$

For the mirrored curve of Fermat's spiral, the following parametrization is proposed:

$$P_{\overline{\text{FS}}}(s) = \begin{bmatrix} x_{\text{end}} - k\sqrt{\theta_{\text{end}}}\,(1-s)\cos\left(-\rho\theta_{\text{end}}(1-s)^2 + \chi_{\text{end}}\right) \\ y_{\text{end}} + k\sqrt{\theta_{\text{end}}}\,(1-s)\sin\left(-\rho\theta_{\text{end}}(1-s)^2 + \chi_{\text{end}}\right) \end{bmatrix},$$

$$s \coloneqq \frac{\sqrt{\theta_{\text{end}} - \theta}}{\sqrt{\theta_{\text{end}}}} \Rightarrow 0 \le s \le 1 \tag{13}$$

where (x_0, y_0) is the starting point, $(x_{\text{end}}, y_{\text{end}})$ is the endpoint, θ is the polar angle, θ_{end} is the polar angle of the endpoint, χ_0 and χ_{end} are the path-tangential angles of Fermat's spiral at the starting and the endpoint, and ρ determines the direction of spiral rotation.

3. Problem Statement

REMUS vehicles are low-cost AUVs designed by the Woods Hole Oceanographic Institution serving in a range of oceanographic applications, such as surveying and mapping. The vehicles are torpedo-shaped and underactuated without lateral thrust; a propeller and fins are used for steering and diving. Besides, the mathematical model of REMUS vehicles has been well researched, which can be used in motion control simulation of underactuated AUVs [20].

This section describes the kinematics and dynamics expressions of the REMUS vehicles and problem formulation of the composite curve path following.

3.1. AUV Model considering Currents. Considering the influences of currents, the kinematics model in the horizontal plane can be expressed in terms of the relative surge and sway velocities [20,21].

$$\begin{aligned} \dot{x} &= u_r\cos(\psi) - v_r\sin(\psi) + V_x, \\ \dot{y} &= u_r\sin(\psi) + v_r\cos(\psi) + V_y, \\ \dot{\psi} &= r. \end{aligned} \tag{14}$$

As depicted in Figure 1, (x) and y are the coordinates of the center of mass of the vehicle expressed in the inertial frame $\{I\}$. ψ and r define its heading angle and yaw velocity. The pair (V_x, V_y) denotes the northeast current velocities in $\{I\}$. Hence, the body-fixed current velocities in surge and sway directions (u_c, v_c) are given by

$$\begin{aligned} u_c &= V_x\cos(\psi) - V_y\sin(\psi), \\ v_c &= V_x\sin(\psi) + V_y\cos(\psi). \end{aligned} \tag{15}$$

The relative surge and sway velocity can be defined as

$$\begin{aligned} u_r &= u - u_c, \\ v_r &= v - v_c, \end{aligned} \tag{16}$$

where u and v are the surge and sway velocity relative to the Earth.

Besides, the relative resultant velocity can be expressed as

$$U_r = \sqrt{u_r^2 + v_r^2}. \tag{17}$$

The REMUS vehicle considered in this paper is based on the following assumptions.

Assumption 1. The vehicle has two axial planes of symmetry, top-bottom and port-starboard symmetry, respectively.

Assumption 2. The vehicle center of gravity is the same as the vehicle center of buoyancy, and the origin of the vehicle body-fixed coordinate system is located at the vehicle center of buoyancy.

Neglecting the motions in heave, roll, and pitch directions, the 3-DOF dynamics model of REMUS vehicle in the horizontal plane can be simplified as

$$\begin{bmatrix} \dot{u}_r \\ \dot{v}_r \\ \dot{r} \end{bmatrix} = \begin{bmatrix} m - X_{\dot{u}} & 0 & 0 \\ 0 & m - Y_{\dot{V}} & -Y_{\dot{r}} \\ 0 & -N_{\dot{v}} & I_{zz} - N_{\dot{r}} \end{bmatrix}^{-1} \begin{bmatrix} \Sigma X \\ \Sigma Y \\ \Sigma N \end{bmatrix}, \tag{18}$$

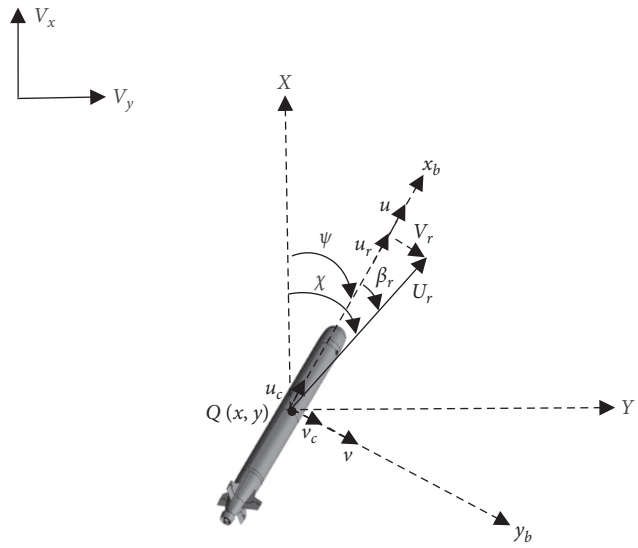

Figure 1: The kinematics description of AUVS in the horizontal plane.

where ΣX and ΣY define the nonacceleration terms along the x-axis and y-axis, and ΣN defines the nonacceleration terms of rotation along the z-axis. The description of ΣX, ΣY, and ΣNcan be shown as

$$\begin{aligned}\Sigma X &= X_{u|u|}u_r|u_r| + X_{vr}v_r r + X_{rr}rr + X_T,\\ \Sigma Y &= Y_{v|v|}v_r|v_r| + Y_{r|r|}r|r| + Y_{ur}u_r r\\ &\quad - mu_r r + Y_{uv}u_r v_r + Y_{uu\delta}u_r^2\delta_r,\\ \Sigma N &= N_{v|v|}v_r|v_r| + N_{r|r|}r|r| + N_{ur}u_r r\\ &\quad + N_{uv}u_r v_r + N_{uu\delta}u_r^2\delta_r,\end{aligned} \tag{19}$$

where u_r, v_r, and r are relative surge, sway, and yaw velocity of the vehicle, which constitute the kinematics status of the vehicle. The thrust X_T and the rudder angle δ_r denote the control input. The symbols similar to $X_{(\cdot)}$, $Y_{(\cdot)}$, and $N_{(\cdot)}$ represent the hydrodynamic parameters of the model, which are used for the calculation of hydrodynamic forces and moments. m represents the mass of the vehicle, and I_{zz} is the moments of inertia. The values of these parameters are presented in Table 2.

3.2. Kinematics Error Description. As depicted in Figure 2, the composite curve path L is composed of two subpaths, L_1 and L_2. Q is the origin of the body-fixed coordinate system of the AUV and P is the virtual point moving along the path. The kinematics error is described in the Frenet–Serret frame $\{F\}$ [22] attached to the point P. However, different from the traditional Frenet–Serret frame $\{F\}$, P is not the closest point on the path to the vehicle, but a point which evolves according to the designed control law. In this way, the singularity caused by parametrization with arc length can also be avoided [23].

The tracking error expressed in $\{F\}$ can be described as

$$\begin{cases} x_e = (x - x_p)\cos(\chi_p) + (y - y_p)\sin(\chi_p),\\ y_e = -(x - x_p)\sin(\chi_p) + (y - y_p)\cos(\chi_p),\end{cases} \tag{20}$$

where x_e is the along-track error and y_e is the cross-track error, (x, y) and (x_p, y_p) are the coordinates of the AUV and the virtual point in the inertial coordinate system, and χ_p is the path-tangential angle of the desired path.

Differentiating (20) yields the error dynamics build in

$$\Sigma_1:\ \begin{cases} \dot{x}_e = -U_p + U_r\cos(\psi + \beta_r - \chi_p) + r_p y_e + \cos(\chi_p)V_x + \sin(\chi_p)V_y,\\ \dot{y}_e = U_r\sin(\psi + \beta_r - \chi_p) - r_p x_e - \sin(\chi_p)V_x + \cos(\chi_p)V_y,\end{cases} \tag{21}$$

where $r_p = \dot{\chi}_p$ is the angular speed of the path and $\beta_r = a\tan 2(v_r, u_r)$ is the drift angle.

Generally, the problem of the composite curve path following for underactuated AUV can be formulated as follows:

Given a constant thrust X_T and desired composite curve path L, select an appropriate way to parametrize the path (1), design guidance and virtual point control laws to generate the desired heading angle ψ_d and realize the global path following, and then develop an active heading controller to

Table 2: Parameters of the REMUS AUV.

Parameter	Value
m	30.48 kg
$X_{u\|u\|}$	$-1.62\,kg/m$
$X_{\dot{u}}$	−0.93 kg
X_{vr}	35.5 kg/rad
X_{rr}	1.93 kg · m/rad
$Y_{v\|v\|}$	−1310 kg/m
$Y_{\dot{v}}$	−35.5 kg
$Y_{r\|r\|}$	0.632 kg · m/rad^2
$Y_{\dot{r}}$	1.93 kg · m/rad
Y_{ur}	5.22 kg/rad
Y_{uv}	28.6 kg/m
$Y_{uu\delta}$	9.64 kg/ (m · rad)
$N_{r\|r\|}$	−9.4 kg · m^2/rad^2
$N_{v\|v\|}$	−3.18 kg
$N_{\dot{v}}$	1.93 kg/m
$N_{\dot{r}}$	−4.88 kg · m^2/rad
N_{ur}	−2.0 kg · m/rad
N_{uv}	−24 kg
$N_{uu\delta}$	−6.15 kg/rad
I_{zz}	3.45 kg · m^2
$X\Gamma$ max	$6.48N$
δ_r max	35°

achieve the expected heading angle, so that the path tracking error can be eliminated.

4. Path following Control Design

To eliminate the tracking error under the influence of unknown static currents, a new path following controller is proposed with cascade structure, as shown in Figure 3.

First, the designed composite curve path is parametrized by a common scalar variable in a continuous way, and a point (P) is selected as the virtual target to be followed. Then, the kinematics error between the coordinates of the AUV and the virtual target point can be calculated including the along-track error and the cross-track error. To eliminate the along-track error, the speed of the virtual point ($\dot{s}$) is introduced as a control input. Besides, utilizing the adaptive ILOS guidance with a current observer, the desired heading angle is given to eliminate the cross-track error. Next, the heading control system (an improved NISM controller) is designed to realize the desired heading angle ($\psi_e = 0$) by controlling the rudder (δ_r) under constant thrust (X_T). Finally, the cascade structure proved to be globally k-exponentially stable under the influence of static currents.

4.1. The AILOS Guidance. The path-tangential speed of the virtual point can be used as a control input [18,23]:

$$U_p = U_r \cos\left(\psi + \beta - \chi_p\right) + kx_e + \cos\left(\chi_p\right)V_x + \sin\left(\chi_p\right)V_y, \tag{22}$$

where $k > 0$ is a gain parameter; the virtual point will move toward the direct projection of the vehicle onto the x-axis of $\{F\}$, whose purpose is to reduce the along-track error to zero.

Substituting (22) into (21) gives

$$\dot{x}_e = -kx_e + r_p y_e. \tag{23}$$

Simultaneously, adaptive ILOS guidance law is used to derive a desired heading angle to eliminate the cross-track error. As illustrated in Figure 1, the desired heading angle is designed as [3]

$$\psi_d = \chi_p + \chi_r - \beta_r, \tag{24}$$

with

$$\chi_r = \arctan\left(-\frac{1}{\Delta}\left(y_e + \alpha\right)\right), \tag{25}$$

where $\Delta > 0$ is the look-ahead distance along the tangential path in $\{F\}$, which is given in meters and usually takes values between 1.5 and 2.5 times the length of a vehicle. Besides, the parameter α is a virtual control input used to compensate for the disturbance of unknown currents.

As the heading error can be expressed as $\psi_e = \psi - \psi_d$, the expression of $\dot{y}_e$ in (21) can be rewritten as

$$\dot{y}_e = U_r \sin\left(\psi_e + \chi_r\right) - r_p x_e - \sin\left(\chi_p\right)V_x + \cos\left(\chi_p\right)V_y. \tag{26}$$

Substituting (25) into (26) gives

$$\begin{aligned}\dot{y}_e = {} & U_r \sin\left(\psi_e + \arctan\left(-\frac{1}{\Delta}\left(y_e + \alpha\right)\right)\right) - r_p x_e \\ & - \sin\left(\chi_p\right)V_x + \cos\left(\chi_p\right)V_y.\end{aligned} \tag{27}$$

Then, (27) can be rewritten as

$$\begin{aligned}\dot{y}_e = {} & -\frac{U_r\left(y_e + \alpha\right)}{\sqrt{\Delta^2 + \left(y_e + \alpha\right)^2}} - r_p x_e - \sin\left(\chi_p\right)V_x + \cos\left(\chi_p\right)V_y \\ & + U_r \phi_1\left(y_e, \psi_e\right)\psi_e,\end{aligned} \tag{28}$$

where

$$\begin{aligned}\phi_1\left(y_e, \tilde{\psi}\right) = {} & \frac{\sin\left(\psi_e\right)}{\psi_e}\frac{\Delta}{\sqrt{\Delta^2 + \left(y_e + \alpha\right)^2}} \\ & - \frac{\cos\left(\psi_e\right) - 1}{\psi_e}\frac{y_e + \alpha}{\sqrt{\Delta^2 + \left(y_e + \alpha\right)^2}}.\end{aligned} \tag{29}$$

To eliminate the influence of the currents, α can be designed as

$$\alpha = \frac{y_e\theta_n^2 + \theta_n\sqrt{\Delta^2\left(1 - \theta_n^2\right) + y_e^2}}{1 - \theta_n^2}, \tag{30}$$

where

$$\theta_n = \frac{-\sin\left(\chi_p\right)V_x + \cos\left(\chi_p\right)V_y}{U_r}. \tag{31}$$

As the currents considered in this paper are much smaller than the speed of the vehicle, it is easy to conclude

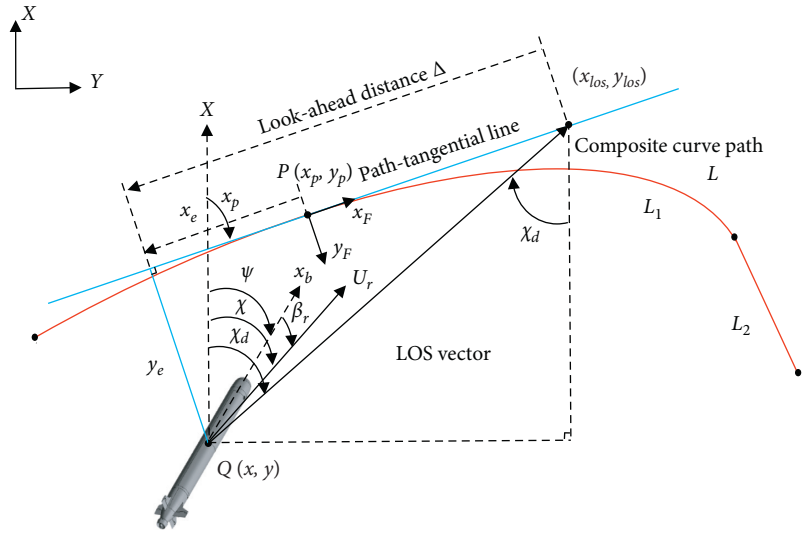

Figure 2: The kinematics description of path following in horizontal plane.

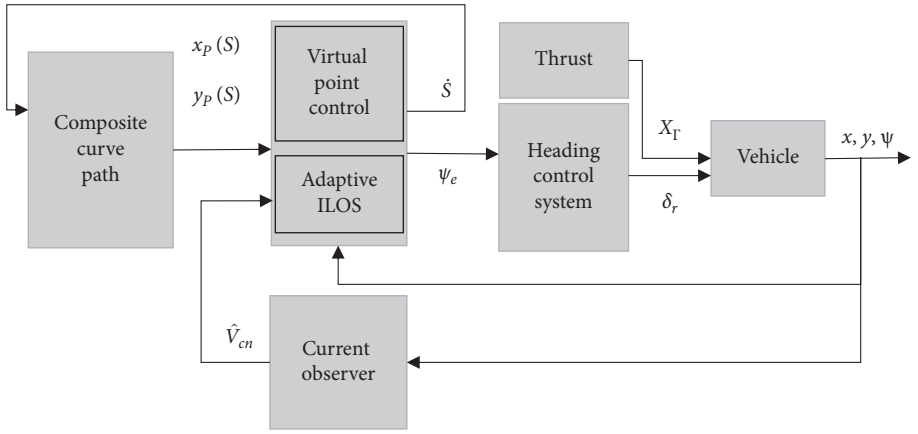

Figure 3: The cascade structures with a current observer.

that $|\theta_n| < 1$. Based on this assumption, there is no singularity in (30).

The first derivative of the kinematics error can be described as

$$\begin{cases} \dot{x}_e = -kx_e + r_p y_e, \\ \dot{y}_e = -\dfrac{U_r y_e}{\sqrt{\Delta^2 + (y_e + \alpha)^2}} - r_p x_e + U_r \phi(y_e, \psi_e)\psi_e. \end{cases} \tag{32}$$

Theorem 1. *Assume that $\psi_e = 0$, $U_r > 0$, $\Delta > 0$, and V_x and V_y are known. Furthermore, assume that U_p is computed using (22) and ψ_d is calculated as (24). Then, the equilibrium point $(x_e, y_e) = (0, 0)$ of the system (32) is globally k-exponentially stable.*

Proof. By substituting $\psi_e = 0$ into (32), the Lyapunov Function Candidate (LFC) $V_1 = (1/2)x_e^2 + (1/2)y_e^2$ has the time derivative

$$\begin{aligned} \dot{V}_1 &= x_e \dot{x}_e + y_e \dot{y}_e \\ &= -kx_e^2 - \frac{U_r y_e^2}{\sqrt{\Delta^2 + (y_e + \alpha)^2}}, \end{aligned} \tag{33}$$

which is negative since $k > 0$ and $U_r > 0$. Hence, the equilibrium point $[x_e, y_e]^2 = 0$ is uniformly globally asymptotically stable (UGAS) and uniformly locally exponentially stable (ULES) or globally k-exponentially stable [24].

However, currents are generally difficult to measure. To eliminate the influence of the unknown currents, the current observer is designed to predict the currents. The currents can be described as $V_{cn} = (V_x, V_y)^T$, and $\hat{V}_{cn}$ is the estimated value of V_{cn}. The position of AUV in $\{I\}$ can be express as $\eta_1 = (x, y)^T$, and $\hat{\eta}_1$ is the estimated value of η_1. According to (14), the derivative of η_1 can be expressed as

$$\dot{\eta}_1 = R(\psi)\nu_{1r} + V_{cn}. \tag{34}$$

Here, $\nu_{1r} = (u_r, v_r)$, and $R(\psi) = \begin{bmatrix} \cos(\psi) & -\sin(\psi) \\ \sin(\psi) & \cos(\psi) \end{bmatrix}$.

The current observer can be designed as [25]

$$\begin{cases} \dot{\widehat{V}}_{cn} = k_{ob1} I_2 (\eta_1 - \widehat{\eta}_1), \\ \dot{\widehat{\eta}}_1 = R(\psi)\nu_{1r} + \widehat{V}_{cn} + k_{ob2} I_2 (\eta_1 - \widehat{\eta}_1), \end{cases} \tag{35}$$

where $\widetilde{\eta}_1 = \eta_1 - \widehat{\eta}_1$ and $\widetilde{V}_{cn} = (V_{cn} - \widehat{V}_{cn})$

Assume that the currents are changing slowly relative to time, which means $\dot{V}_{cn} = 0$. Substituting (34) to (35) gives

$$\underbrace{\begin{bmatrix} \dot{\widetilde{V}}_{cn} \\ \dot{\widetilde{\eta}}_1 \end{bmatrix}}_{\dot{X}} = \underbrace{\begin{bmatrix} 0 & -k_{ob1} I_2 \\ I_2 & -k_{ob2} I_2 \end{bmatrix}}_{\mathbf{A}} \underbrace{\begin{bmatrix} \widetilde{V}_{cn} \\ \widetilde{\eta}_1 \end{bmatrix}}_{\mathbf{X}}, \tag{36}$$

where $k_{ob1} > 0$, $k_{ob2} > 0$. □

Theorem 2. *The current observer (36) is globally exponentially stable (GES) for static currents.*

Proof. Consider the following Lyapunov function candidate:

$$V_2 = \mathbf{X}^T \mathbf{P} \mathbf{X}, \tag{37}$$

where $\mathbf{X} = [\widetilde{V}_{cn}, \widetilde{\eta}_1]$; $\mathbf{P} = \mathbf{P}^T > 0$ is given by

$$\mathbf{P}\mathbf{A} + \mathbf{A}^T \mathbf{P} = -q\mathbf{I}_4, \tag{38}$$

where $q > 0$. Substitution of (36) into (38) gives

$$\mathbf{P} = \begin{bmatrix} q\dfrac{k_{ob1} + k_{ob2}^2 + 1}{2k_{ob1}k_{ob2}} I_2 & -\dfrac{1}{2} q I_2 \\ -\dfrac{1}{2} q I_2 & q\dfrac{k_{ob1} + 1}{2k_{ob2}} I_2 \end{bmatrix}. \tag{39}$$

When $k_{ob1} > 0$ and $k_{ob2} > 0$, it can be seen that the leading principal minors of $\mathbf{P}$ are positive. Hence, V_2 is positive definite.

The time derivative of V_2 is

$$\dot{V}_2 = \dot{X}^T \mathbf{P} \mathbf{X} + \mathbf{X}^T \mathbf{P} \dot{X}. \tag{40}$$

Substituting of (36) and (38) into (40) gives

$$\dot{V}_2 = -q\|\mathbf{X}\|^2. \tag{41}$$

Consequently, the equilibrium point $[\widetilde{V}_{cn}, \widetilde{\eta}_1]^T = 0$ is GES, according to Theorem 4.10 in [26]. □

4.2. Subpath Switching Algorithm. The path-tangential speed U_P of the virtual point is used as a control input to stabilize the along-track error. Moreover, according to (6), the first derivative of the parameter s of the virtual point w.r.t. time can be expressed as

$$\dot{s} = \frac{U_P}{\sqrt{x_p'(s)^2 + y_p'(s)^2}}. \tag{42}$$

It can be seen that $\dot{s}$ is singularity-free for all regular paths. Besides, the value of $\dot{s}$ is dependent on U_P and the parametrization of curves. As the composite curve path usually does not satisfy C^1 continuity, and each curve segment is parametrized differently, $\dot{s}$ is discontinuous at the waypoint.

Besides, as each curve segment with different characteristics is parametrized with the same parameter interval, the length of the curve segments will have a significant impact on the value of $\dot{s}$. Relatively, the equal amount of $\dot{s}$ will have a different meaning for different curve segments. Hence, the switching algorithm has to be considered for path following of the composite curve path, especially when the length of subpaths varies a lot.

The parameter s of the virtual point can be obtained from the numerical integration of $\dot{s}$. It can be expressed in Euler's method:

$$s_{k+1} = s_k + \dot{s}_k \Delta t = s_k + \Delta s_k. \tag{43}$$

When $s_k + \Delta s_k >= i$, the reference point will switch to the L_{i+1} subpath from the L_i curve segments. Considering the different effect of $\dot{s}$ for two curve segments, at this time, s_{k+1} cannot be calculated by (43) directly. The problem can be solved by setting $s_{k+1} = i$, which is the parameter of the starting point of L_{i+1} subpath, as the displacement of the reference point in a period is small and has little impact on the path following. Ultimately, the global path following for composite curve path can be achieved.

Besides, an additional path switching mechanism can be introduced to achieve better tracking effect at path switching, especially for the piecewise linear path with G^0 continuity. As shown in Figure 4, it is suggested that a so-called circle of acceptance is associated with each waypoint connecting two subpaths [8]. The switching criterion can be defined as

$$\left(x_{p_k} - x\right)^2 + \left(y_{p_k} - y\right)^2 \le R_k^2, \tag{44}$$

where R_k is the radius of the circle of acceptance. The magnitude of R_k can be determined by considering the turning ability of the AUV. Generally, the parameter $R_k$can be selected as $R_k \le \Delta$. After the criterion has been satisfied, the next curve segment will be followed.

Generally, for composite curve path following, each subpath switching can be regarded as the beginning of tracking a new path initialized by the current state of the AUV.

4.3. Heading Controller Design. To obtain the desired heading angle given by the guidance law, the heading control system is designed to make the heading error converge to zero.

A non-model-based NISM control algorithm is utilized to realize the heading control. The nonlinear sliding surfaces are designed as

$$\begin{cases} \sigma_1(\psi_e) = k_1 \tanh(k_2 \psi_e) + \dot{\psi}_e, \\ \sigma_2(\sigma_1) = k_3 \tanh(k_4 \sigma_1) + \dot{\sigma}_1, \end{cases} \tag{45}$$

where $k_i > 0 (i = 0, 1, \ldots, 4)$ are the control parameters, $\tanh(x)$ is a strictly bounded nonlinear hyperbolic tangent function, and σ_1 and σ_2 are designed slide mode surfaces.

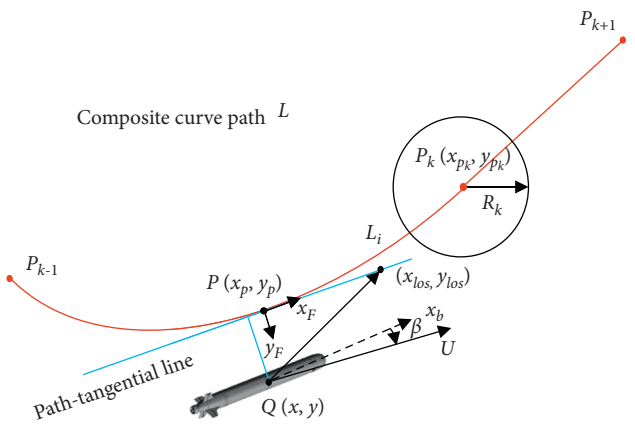

FIGURE 4: The subpath switching algorithm of the composite curve path.

To stabilize σ_1 and σ_2, the incremental feedback control law is designed as

$$\dot{\delta}_r = k_p \tanh(k_5\sigma_2) + k_s \operatorname{sgn}(\sigma_2), \tag{46}$$

where $\dot{\delta}_r$ is the derivative of the rudder angle.

Different from the standard NISM controller [27], $\tanh(x)$ is used for the incremental feedback calculation of $\dot{\delta}_r$. By considering the discontinuity of the connection point between two curve segments, the value of σ_2 may become very large suddenly. This will cause excessive rudder speed which is not practical and may cause damage to the rudder system. Hence, in (46), k_p can be used to limit the maximum rudder speed. When there is time-varying interference, k_s can be set to a smaller value to ensure the stability of the control system. The signs of k_p and k_s are selected relating to the definition of the rudder. For the model of the REMUS vehicle, the rudder angle is defined as positive, when the resulting force causes the vehicle to turn left. Hence, k_p and k_s are selected to be positive. In addition, k_5 is also selected to be positive, which is used to adjust the range of coordinate where $\dot{\delta}_r$ is varying at an exponential rate.

According to (45), when $\sigma_2 = 0$, one can obtain

$$\dot{\sigma}_1 = -k_3 \tanh(k_4\sigma_1). \tag{47}$$

Hence,$\sigma_1 \longrightarrow 0$. Similarly, when $\sigma_1 = 0$, one can obtain

$$\dot{\psi}_e = -k_1 \tanh(k_2\psi_e). \tag{48}$$

Hence, $\psi_e \longrightarrow 0$. This means that the heading error will converge to zero when $\sigma_2 = 0$. According to (47) and (48) and the properties of the hyperbolic function, it can be known that when $k_4\sigma_1$ and $k_2\psi_e$ are large, σ_1 and ψ_e will tend to zero at a fixed rate. Moreover, when $k_4\sigma_1$ and $k_2\psi_e$ are small, σ_1 and ψ_e will exponentially converge to zero. Besides, k_3 and k_1 determine the maximum attenuation rate of σ_1 and ψ_e, and k_4 and k_2 are used to adjust the range of coordinate where σ_1 and ψ_e are decaying at an exponential rate.

Theorem 3. *Assume that the sliding mode surfaces (45) and the incremental feedback control law (46) are used for the heading autopilot system, the definition of the sign of the rudder is known* $((\partial\dot{r}/\partial\delta_r) < 0)$*, and* $k_p > 0$*,* $k_s \geq 0$*; then, the equilibrium point* $\psi_e = 0$ *is globally k-exponentially stable.*

Proof. The Lyapunov Function Candidate (LFC) $V_3 = (1/2)\sigma_2^2$ has the time derivative

$$\dot{V}_3 = \sigma_2 \frac{\partial\sigma_2}{\partial\delta_r}\dot{\delta}_r. \tag{49}$$

According to (45),

$$\sigma_2(\sigma_1) = k_3 \tanh(k_4\sigma_1) + k_1k_2r_e \sec^2(k_2\psi_e) + \dot{r}_e, \tag{50}$$

where $r_e = r - r_d$. According to (18) and (19) and the parameters of the REMUS AUV, ignoring the variables independent of δ_r, one can obtain

$$\frac{\partial\sigma_2}{\partial\delta_r} = \frac{\partial\dot{r}}{\partial\delta_r} < 0. \tag{51}$$

According to (45), it can be known that

$$\sigma_2\dot{\delta}_r = k_p\sigma_2 \tanh(k_5\sigma_2) + k_s|\sigma_2| \geq k_p\sigma_2 \tanh(k_5\sigma_2) \geq 0. \tag{52}$$

Hence, it can be derived that

$$\dot{V}_3 \leq k_p\sigma_2 \tanh(k_5\sigma_2)\frac{\partial\sigma_2}{\partial\delta_r} \leq 0. \tag{53}$$

Depending on the properties of the hyperbolic function and Lyapunov stability theory, it can be concluded that $\sigma_2 = 0$ is UGAS and ULES or globally k-exponentially stable. Similarly, according to (47) and (48), $\psi_e = 0$ is globally k-exponentially stable. □

4.4. Stability of the Cascade System. Consider the following cascade system:

$$\begin{cases} \dot{x}_{pt} = f_1(t, x_{pt}) + g(t, x_{pt}, y_{pt})y_{pt}, \\ \dot{y}_{pt} = f_2(t, y_{pt}). \end{cases} \tag{54}$$

System (54) can be regarded as

$$\sum_{1pt}: \ \dot{x}_{pt} = f_1(t, x_{pt}), \tag{55}$$

which is perturbed by the output of the system

$$\sum_{2pt}: \ \dot{y}_{pt} = f_2(t, y_{pt}). \tag{56}$$

Besides, the theorems proposed by [13] can be used to prove the stability of the cascade system. To be convenient, the theorems are presented here.

Theorem 4. *Cascaded system (54) is GUAS if the following three assumptions hold:*

(i) Assumption on $\sum_{1pt}$: the system $f_1(t, x_{pt})$ is GUAS and there exists a continuously differentiable function $V(t, x_{pt})$: $IR_{\geq 0} \times IR^n \longrightarrow IR$ that satisfies

$$W_x \leq V\left(t, x_{pt}\right),$$
$$\frac{\partial V}{\partial t} + \frac{\partial V}{\partial x_{pt}} \cdot f_1\left(t, x_{pt}\right) \leq 0, \quad \forall \left\| x_{pt} \right\| \geq \eta_{pt}, \tag{57}$$
$$\left\| \frac{\partial V}{\partial x_{pt}} \right\| \cdot \left\| x_{pt} \right\| \leq c_{pt} V\left(t, x_{pt}\right) 0, \quad \forall \left\| x_{pt} \right\| \geq \eta_{pt},$$

where W_x is a positive definite proper function and $c_{pt} > 0$ and $\eta_{pt} > 0$ are constants.

(ii) Assumption on the interconnection: the function $g(t, x_{pt}, y_{pt})$ satisfies for all $t \geq t_0$

$$\left\| g\left(t, x_{pt}, y_{pt}\right) \right\| \leq \theta_1\left(\left\| y_{pt} \right\| \right) + \theta_2\left(\left\| y_{pt} \right\| \right) \left\| x_{pt} \right\|, \tag{58}$$

where θ_1, θ_2: $IR_{\geq 0} \longrightarrow IR_{\geq 0}$ are continuous functions.

(iii) Assumption on $\sum_{2pt}$: the system $\sum_{2pt}$ is GUAS and for all $t_0 \geq 0$

$$\int_{t_0}^{\infty} \left\| y_{pt}\left(t, t_0, y_{pt}\left(t_0\right)\right) \right\| \mathrm{d}t \leq \kappa y_{pt}\left(\left\| t_0 \right\| \right), \tag{59}$$

where the function $\kappa(\cdot)$ is a class κ function [24].

Theorem 5. *In addition to the assumptions in Theorem 4, if both $\sum_{1pt}$ and $\sum_{2pt}$ are globally κ-exponentially stable, then cascaded system (54) is globally κ-exponentially stable.*

For path following under the disturbance of unknown static currents, the stability of cascade system can be proved in two steps. First, without considering the currents, the cascade system described in Theorem 6 can prove to be globally κ-exponentially stable. Then, based on Theorem 6, the cascade system including a current observer can prove to be globally κ-exponentially stable under the influence of unknown static currents.

Theorem 6. *Without considering the currents, the guidance system expressed as (32) and the heading control system described by (45) and (56) can be analyzed as a cascade structure, which is globally κ-exponentially stable at $(x_e, y_e, \psi_e) = (0, 0, 0)$.*

Proof. The cascade can be described as

$$\Sigma_1^1: \begin{cases} \dot{x}_e = -k_1 x_e + r_p y_e, \\ \dot{y}_e = -\dfrac{U_r y_e}{\sqrt{\Delta^2 + \left(y_e + \alpha\right)^2}} - r_p x_e + U_r \phi\left(y_e, \psi_e\right) \psi_e, \end{cases} \tag{60}$$

$$\Sigma_2^1: \dot{\psi}_e = f_1\left(t, \psi_e\right), \tag{61}$$

where $\dot{\psi}_e = f_1(t, \psi_e)$ define the heading error dynamics corresponding to (45).

To prove Theorem 6, the three assumptions in Theorem 4 need to be verified. The nominal system of Σ_1^1 (when $\psi_e = 0$) is

$$\Sigma_{1^*}^1: \begin{cases} \dot{x}_e = -k_1 x_e + r_p y_e, \\ \dot{y}_e = -\dfrac{U_r y_e}{\sqrt{\Delta^2 + \left(y_e + \alpha\right)^2}} - r_p x_e. \end{cases} \tag{62}$$

The LFC is selected as $V_1 = (1/2)x_e^2 + (1/2)y_e^2$, and, according to (33), it is known that $\dot{V}_1 \leq 0$. Hence, the assumption on $\sum_{1*}$ is always satisfied when $c \geq 2$.

Besides, the interconnection term satisfies $|\phi(y_e, \widetilde{\psi})| < = c$, and $c = 1.73$ is the upper bound [12]. Hence, the assumption on the interconnection is also satisfied.

As Σ_2^1 is globally*k*-exponentially stable, the last assumption is also satisfied. Hence, all conditions of Theorem 4 and Theorem 5 are satisfied, and the cascade system is globally *k*-exponentially stable.

Considering the prediction error of observer, the cascade structure can be described as

$$\Sigma_1^2: \begin{cases} \dot{x}_e = -k_1 x_e + r_p y_e + \phi_2\left(\widetilde{V}_{cn}\right), \\ \dot{y}_e = -\dfrac{U_r y_e}{\sqrt{\Delta^2 + \left(y_e + \alpha\right)^2}} - r_p x_e + U_r \phi\left(y_e, \psi_e\right) \psi_e + \phi_3\left(\widetilde{V}_{cn}\right), \\ \dot{\psi}_e = f_1\left(\psi_e\right), \end{cases}$$
$$\Sigma_2^2: \dot{\widetilde{V}}_{cn} = f_2\left(\widetilde{V}_{cn}\right), \tag{63}$$

where

$$\begin{aligned} \phi_2\left(\widetilde{V}_{cn}\right) &= \cos\left(\chi_p\right) \widetilde{V}_x + \sin\left(\chi_p\right) \widetilde{V}_y, \\ \phi_3\left(\widetilde{V}_{cn}\right) &= -\sin\left(\chi_p\right) \widetilde{V}_x + \cos\left(\chi_p\right) \widetilde{V}_y. \end{aligned} \tag{64}$$

□

Theorem 7. *Assume that the currents are changing slowly relative to time and the current observer is designed as (35); by considering the prediction error, the guidance and heading control system expressed as (60) and (61) can be cascaded with the current observer, and the cascade structure is globally k-exponentially stable.*

Proof. The nominal system (Σ_1^2 system with $\widetilde{V}_{cn} = 0$) has proved to be globally k-exponentially stable in Theorem 6. Hence, according to converse Lyapunov theory in [26], there exists Lyapunov function $V_4 = (x_e, y_e, \psi_e)$ that satisfies the assumption on the nominal system. Besides, as the trigonometric functions are strictly bounded and the $\widetilde{V}_{cn}$ is bounded, it can be concluded that $\phi_2(\widetilde{V}_{cn})$ and $\phi_3(\widetilde{V}_{cn})$ are bounded. Moreover, the current observer is GES. Hence, all conditions of Theorem 4 and Theorem 5 are satisfied, and the cascade system is globally k-exponentially stable. □

5. Simulation Results

To verify the effectiveness of the control system for the composite curve path following, three simulation cases are carried out. Case 1 is implemented to verify the performance of the proposed path following controller for the composite curve path without currents. Besides, the PID control and the conventional sliding mode control are introduced as the heading controller to be compared with the improved NISM controller. Based on Case 1, Case 2 is carried out to prove the effectiveness of the additional subpath switching algorithm. In Case 3, unknown static currents are introduced to test the anti-interference ability of the controller based on the current observer.

The composite curve path is designed to contain G0, G1, and G2 continuity at the same time and is composed of seven subpaths, including straight lines, circular arcs, and Fermat's spirals. The parameters of the composite curve path and the controller are shown in Tables 3 and 4. As most parameters of the guidance and heading control system have a clear physical meaning, the parameters are based on hand tuning. The values of the look-ahead distance Δ and the heading control parameter k_p have obvious influence on the control effect and can also be adjusted automatically. Relevant methods can be found in [3, 16].

5.1. Case 1: Path following without Currents. For path following with no currents, $V_x = 0$ and $V_y = 0$. Due to the cascade structure design, the adaptive integral guidance law can be flexibly combined with heading controllers to achieve the desired path tracking. The PID control and conventional sliding mode control [12] are introduced as the heading controller to be compared with the improved NISM controller. The desired composite path and the trajectory of path following are shown in Figure 5. It can be concluded that, by the path parametrization according to (1) and the control of virtual point as (24), the global path planning for composite curve path can be realized.

As shown in Figure 6, compared with the PID control and conventional sliding mode control, the NISM control has faster convergence speed and smaller steady-state error. Besides, the NISM control adopts the incremental feedback control law, which is not based on the model parameters. Hence, it is not easily affected by the uncertainty of the model parameters. In Figure 7, after modifying the value of the hydrodynamic parameter $N_{uu\delta}$ from −6.15 to −4.15, the NISM control can still maintain the heading control, while the conventional sliding mode control produces control error.

Table 3: Parameters of the composite curve path.

No.	Subpath type	Parameter	Value
1	Straight line	(x_0, y_0)	$(-20, 20)$
		L	$200\sqrt{2}$
		χ_l	$\pi/4$
2	Straight line	(x_0, y_0)	$(180, 220)$
		L	200
		χ_l	$\pi/2$
3	Circular arc	(c_{x0}, c_{y0})	$(80, 420)$
		R	100
		α_0	0
		α_1	π
4	Straight line	(x_0, y_0)	$(-20, 420)$
		L	154.9566
		χ_l	$-\pi/2$
5\6	Fermat's spiral	(x_0, y_0)	$(-20, 265.0434)$
		$(x_{\text{end}}, y_{\text{end}})$	$(0, 0)$
		θ_{end}	0.1329
		χ_0	$-\pi/2$
		χ_{end}	$-\pi/4$
		ρ	1
7	Straight line	(x_0, y_0)	$(11.8505, 188.1495)$
		L	237.7993
		χ_l	$-\pi/4$

Table 4: Parameters of the guidance and control system.

Parameter	Value
Δ	6
k	1
k_1	0.8
k_2	1.5
k_3	0.8
k_4	1
k_5	15
k_p	0.1745
k_s	0
X_Γ	$6.48N$
k_{ob1}	1
k_{ob2}	1
R_k	6

The degree of the GC has a high impact on the control of path following. Comparatively, G_1 and G_2 paths have less effect on the path following. However, for G_0 paths, there will be an apparent deviation due to the sudden change of the desired heading angle ψ_d. Hence, G_0 paths are not suitable for path following of underactuated vehicle, and an additional path switching mechanism (44) is required to handle this problem.

The discontinuity of the connection point between two curve segments will cause excessive rudder speed which is not practical and may cause damage to the rudder system. Strictly bounded nonlinear hyperbolic tangent function is used in the NISM control, and the parameter k_p can be used to limit the maximum rudder speed. In Figure 8, the rudder

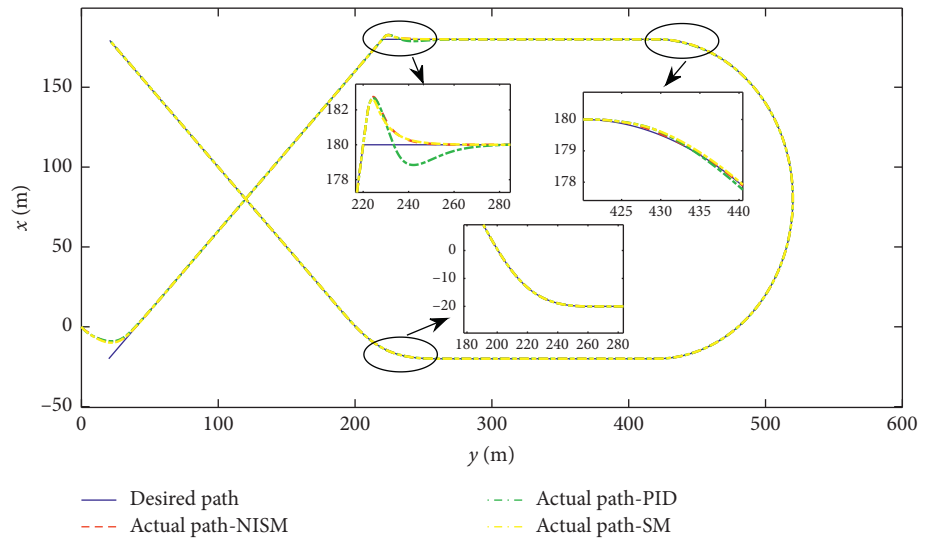

Figure 5: The planned composite curve path and the actual trajectory.

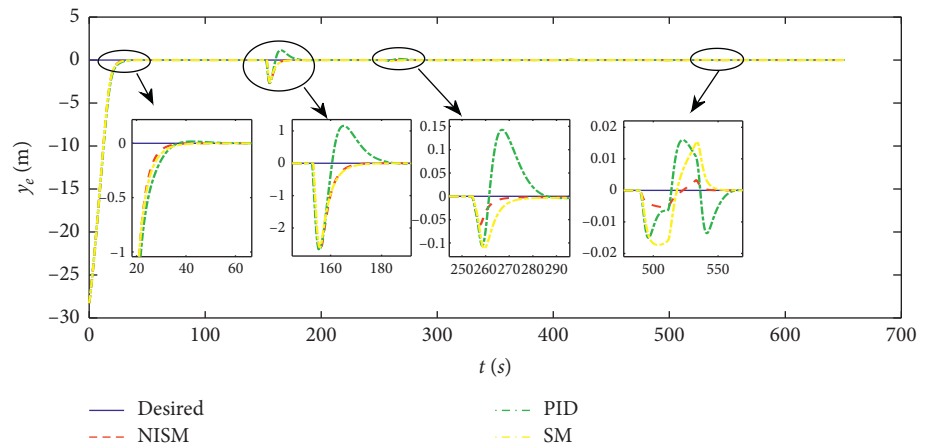

(a)

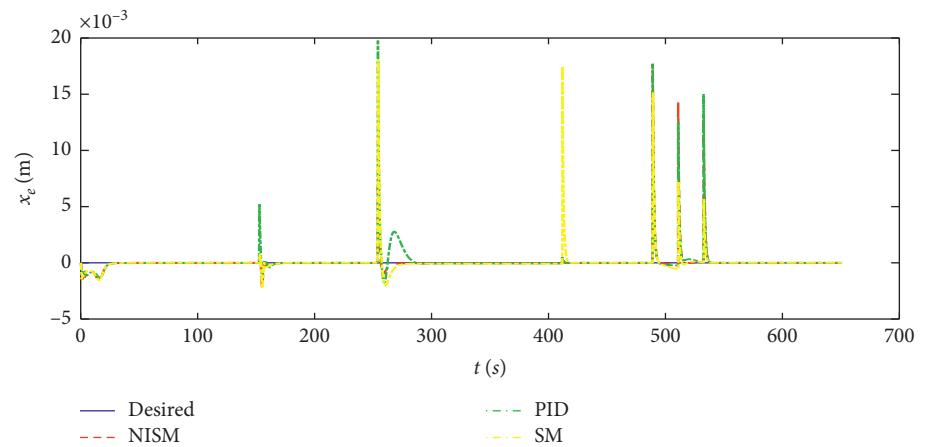

(b)

Figure 6: Continued.

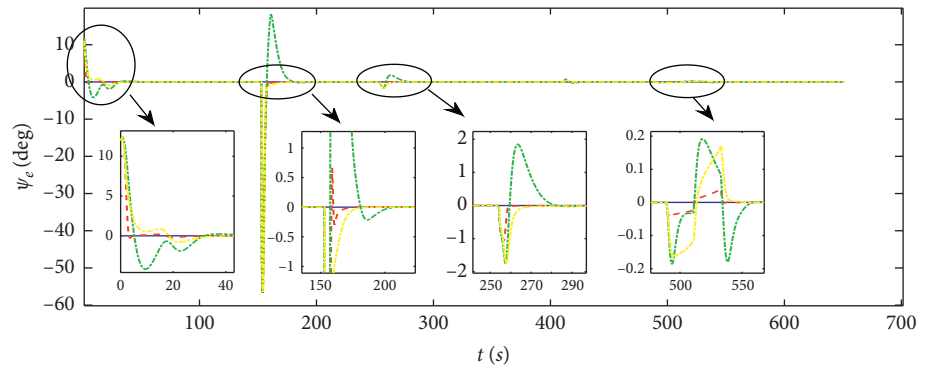

(c)

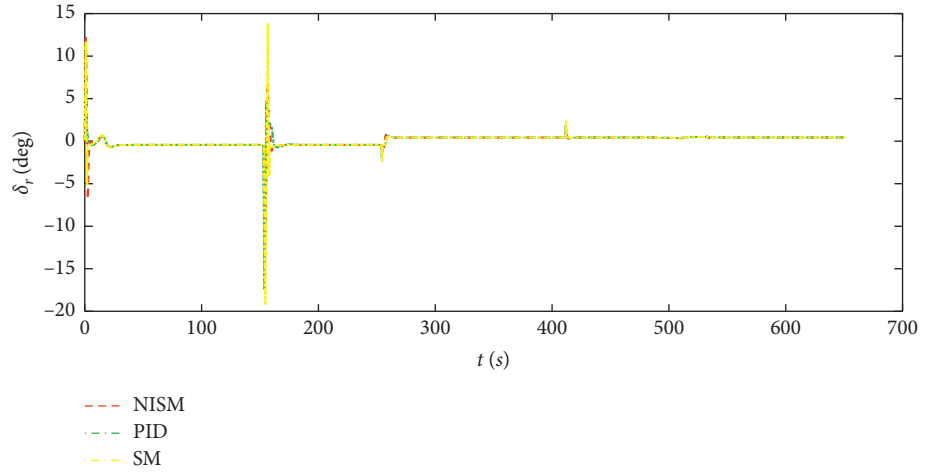

(d)

Figure 6: The tracking error and the heading control error without currents.

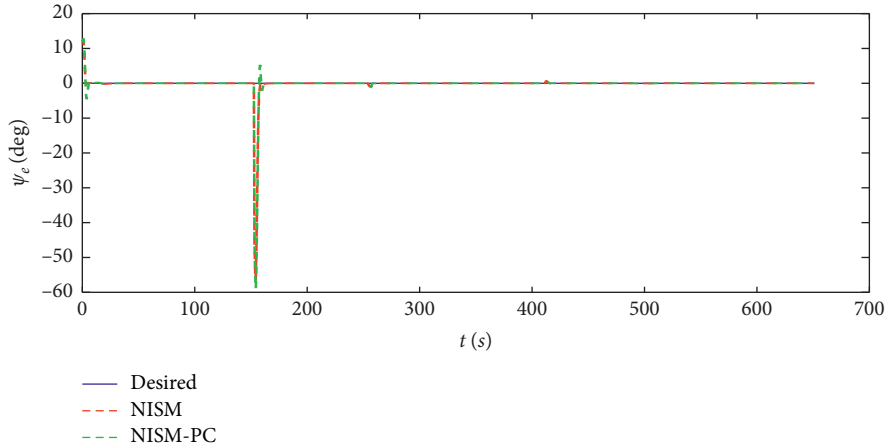

(a)

Figure 7: Continued.

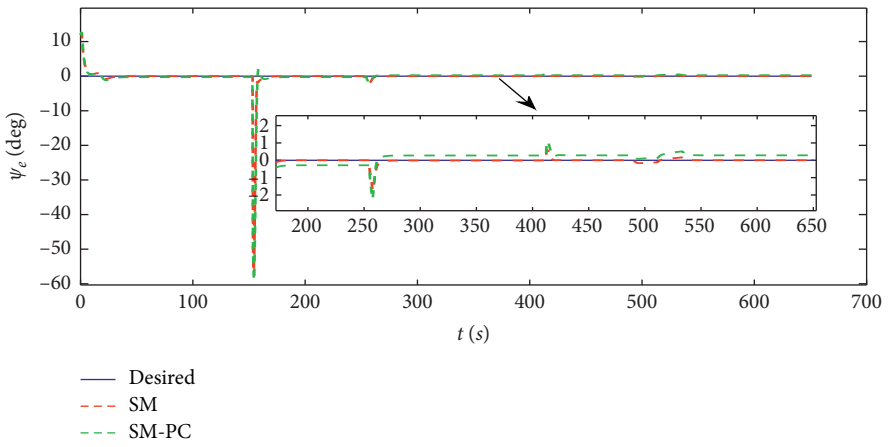

(b)

Figure 7: The comparison of the heading control effect after changing the model parameter.

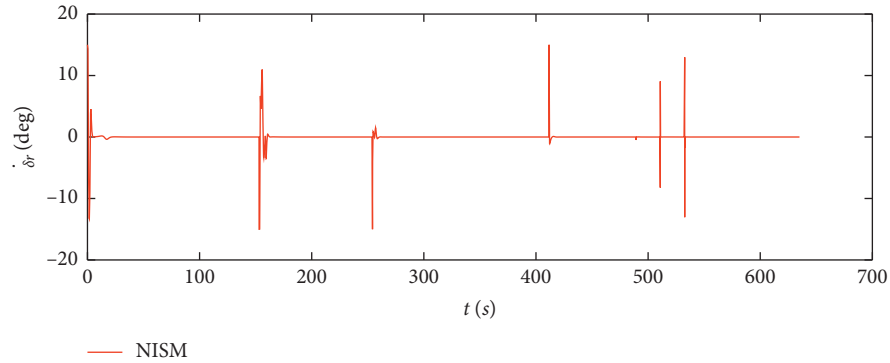

Figure 8: The rudder control of the NISM controller.

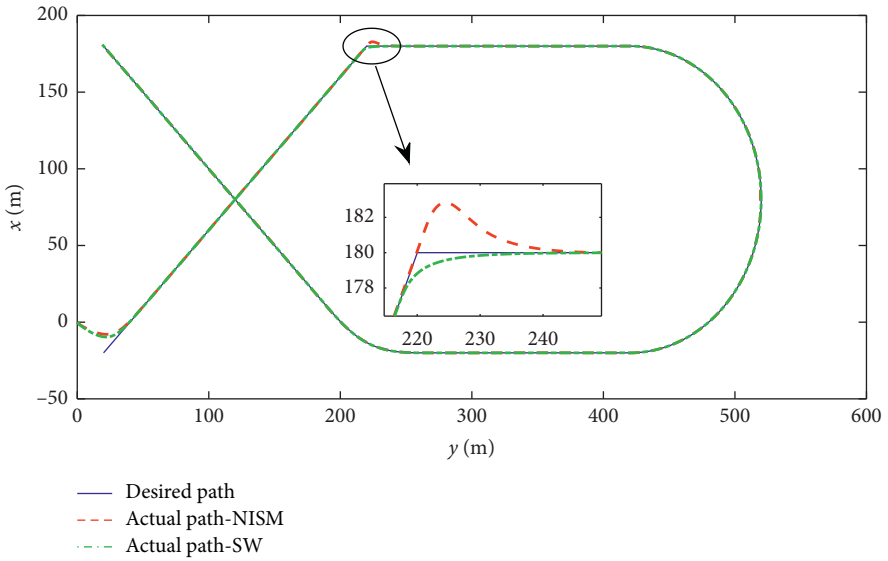

Figure 9: The planned composite curve path and the actual trajectory.

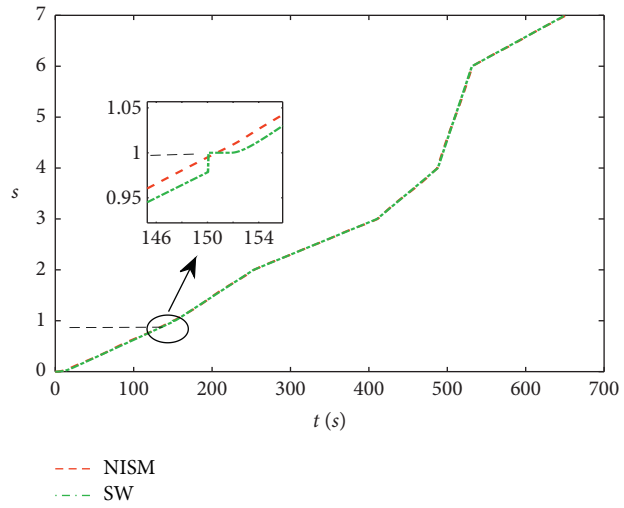

Figure 10: The parameter value of the virtual point.

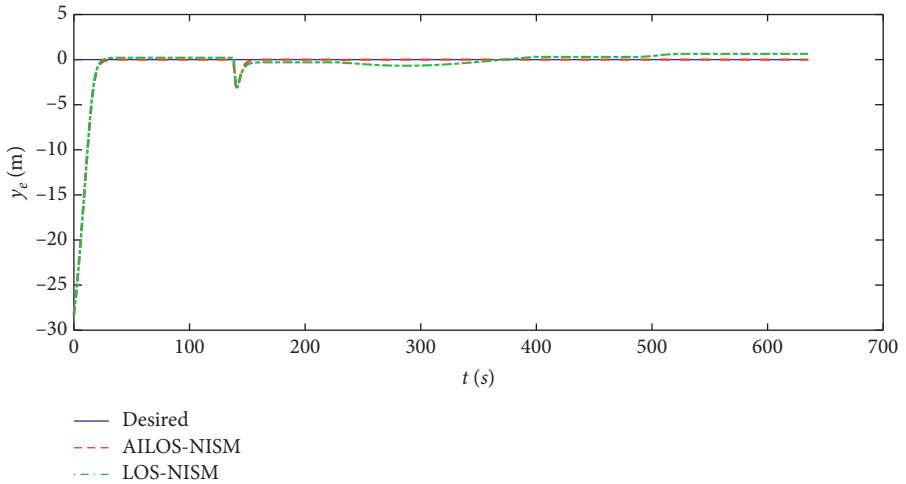

(a)

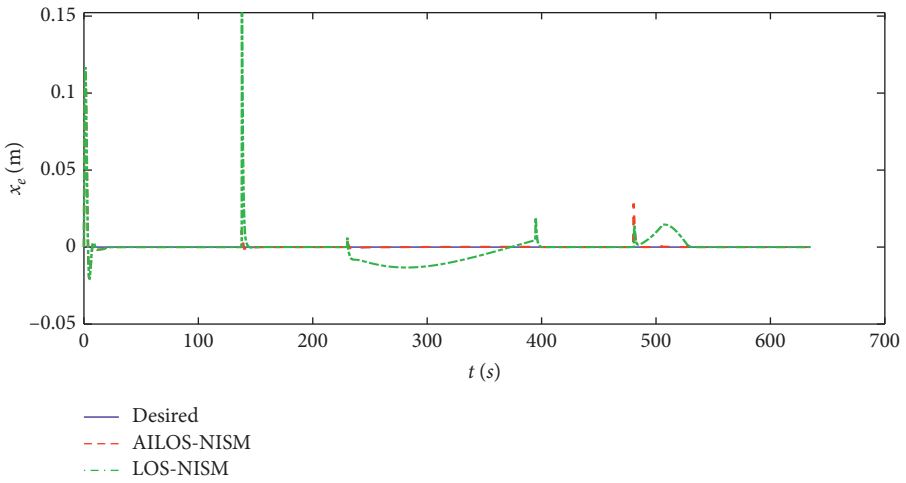

(b)

Figure 11: The tracking error under constant currents.

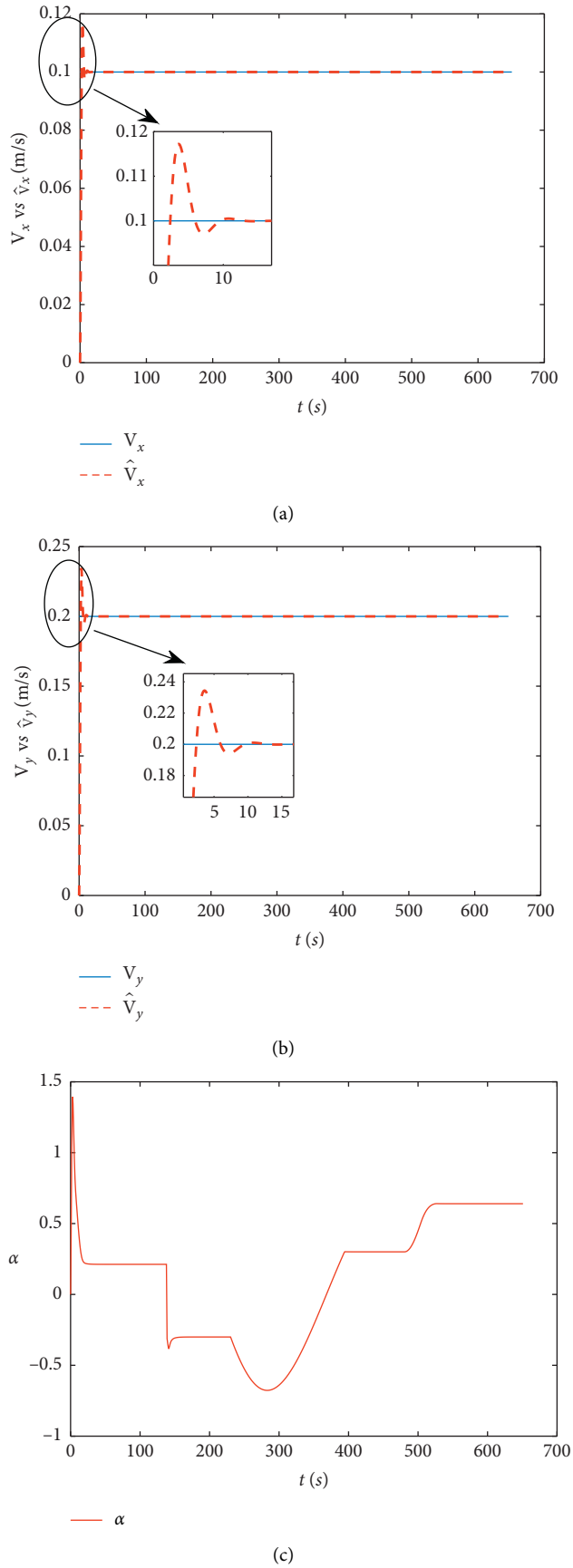

Figure 12: The estimate of constant currents and the compensation coefficient.

speed is limited to 15°/s. Hence, the proposed NISM control is more suitable for the composite curve path following.

5.2. Case 2: Subpath Switching Algorithm. From Case 1, it is known that the tracking trajectory deviates from the desired path obviously at the switching point due to the sudden change of the heading angle for G_0 paths. Hence, in Case 2, an additional path switching mechanism (44) is used to handle this problem.

As shown in Figures 9 and 10, after using the additional path switching algorithm, the vehicle will track the next subpath early near the connection point when the switching criterion is satisfied. In addition, in this way, the tracking error between two subpaths can be reduced obviously.

5.3. Case 3: Path following Unknown Static Currents. For path following with static currents, V_x and V_y are constant values, where V_x is 0.1 (m/s) and V_y is 0.2 (m/s). The simulation results are as follows.

From Figure 11, we can see that, without the current observer, the path following controller will produce certain tracking error under the disturbance of unknown current especially for the curve paths. Besides, from Figure 12, it can be concluded that the currents can be well estimated by the designed observer. Then, the influence of currents can be eliminated at the kinematics level with U_p and α calculated as (22) and (30). Finally, by the cascade structure composed of AILOS guidance and the improved NISM controller, the vehicle can converge to and move along the desired composite curve path.

6. Conclusion

This paper addresses the problems of composite curve path following for an underactuated AUV in the horizontal plane. The global path following of the composite curve path is realized by the virtual point control and the subpath switching algorithm after the parametrization of the composite curve and description of the kinematics error. Besides, the cascade structure composed of AILOS guidance and the improved NISM control proved to be UGAS under the influence of constant currents. Future work will expand the application of the composite curve path following to three-dimensional space.

Data Availability

Partial data used to support the findings of this study are available from the corresponding author upon request.

Conflicts of Interest

The authors declare that there are no conflicts of interest regarding the publication of this paper.

Acknowledgments

This work was supported in part by the National Natural Science Foundation of China (Grant no. 52001132) and Special Funds for Basic Scientific Research in Central Universities of China (Grant no. 2662020GXQD003).

References

[1] C. Yu, C. Liu, L. Lian, X. Xiang, and Z. Zeng, "ELOS-based path following control for underactuated surface vehicles with actuator dynamics," *Ocean Engineering*, vol. 187, p. 106139, 2019.

[2] J. Nie and X. Lin, "Improved adaptive integral line-of-sight guidance law and adaptive fuzzy path following control for underactuated MSV," *ISA Transactions*, vol. 94, pp. 151–163, 2019.

[3] A. M. Lekkas and T. I. Fossen, "Integral LOS path following for curved paths based on a monotone cubic hermite spline parametrization," *IEEE Transactions on Control Systems Technology*, vol. 22, no. 6, pp. 2287–2301, 2014.

[4] Z. Zeng, L. Lian, K. Sammut, F. He, Y. Tang, and A. Lammas, "A survey on path planning for persistent autonomy of autonomous underwater vehicles," *Ocean Engineering*, vol. 110, pp. 303–313, 2015.

[5] Y. A. Kapitanyuk and S. A. Chepinsky, "Control of mobile robot following a piecewise-smooth path," *Gyroscopy and Navigation*, vol. 4, no. 4, pp. 198–203, 2013.

[6] T. I. Fossen, K. Y. Pettersen, and R. Galeazzi, "Line-of-Sight path following for Dubins paths with adaptive sideslip compensation of drift forces," *IEEE Transactions on Control Systems Technology*, vol. 23, no. 2, pp. 820–827, 2015.

[7] L. Liu, D. Wang, and Z. Peng, "Path following of marine surface vehicles with dynamical uncertainty and time-varying ocean disturbances," *Neurocomputing*, vol. 173, pp. 799–808, 2016.

[8] T. I. Fossen, M. Breivik, and R. Skjetne, "Line-of-sight path following of underactuated marine craft," *IFAC Proceedings Volumes*, vol. 36, no. 21, pp. 211–216, 2003.

[9] A. J. Healey and D. B. Marco, "Slow speed flight control of autonomous underwater vehicles: experimental results with NPS AUV II," *Isope*, vol. 11, 1992.

[10] E. Borhaug and K. Y. Pettersen, "Cross-track control for underactuated autonomous vehicles," in *Proceedings of the 44th IEEE Conference on Decision and Control*, pp. 602–608, Seville, Spain, December 2005.

[11] E. Borhaug, A. Pavlov, and K. Y. Pettersen, "Integral LOS control for path following of underactuated marine surface vessels in the presence of constant ocean currents," in *Proceedings of the 2008 47th IEEE Conference on Decision and Control*, pp. 4984–4991, Cancun, Mexico, December 2008.

[12] T. I. Fossen and A. M. Lekkas, "Direct and indirect adaptive integral line-of-sight path-following controllers for marine craft exposed to ocean currents," *International Journal of Adaptive Control and Signal Processing*, vol. 31, no. 4, pp. 445–463, 2017.

[13] E. Panteley, E. Lefeber, A. Loria, and H. Nijmeijer, "Exponential tracking control of a mobile car using a cascaded approach," *IFAC Proceedings Volumes*, vol. 31, no. 27, pp. 201–206, 1998.

[14] Y. Xia, K. Xu, W. Wang, G. Xu, X. Xiang, and Y. Li, "Optimal robust trajectory tracking control of a *X*-rudder AUV with velocity sensor failures and uncertainties," *Ocean Engineering*, vol. 198, p. 106949, 2020.

[15] K. Shojaei and M. Dolatshahi, "Line-of-sight target tracking control of underactuated autonomous underwater vehicles," *Ocean Engineering*, vol. 133, pp. 244–252, 2017.

[16] G. Wang, G. Xu, G. Liu, W. Wang, and B. Li, "Fuzzy iterative sliding mode control applied for path following of an autonomous underwater vehicle with large inertia," *Mathematical Problems in Engineering*, vol. 2019, Article ID 8650243, 14 pages, 2019.

[17] R. Skjetne, *The Maneuvering Problem*, Norwegian University of Science and Technology, Trondheim, Norway, 2005.

[18] M. Breivik and T. I. Fossen, *Guidance Laws for Autonomous Underwater Vehicles*, Springer, Berlin, Germany, 2009.

[19] A. M. Lekkas, *Guidance and Path-Planning Systems for Autonomous Vehicles*, Norwegian University of Science and Technology, Trondheim, Norway, 2014.

[20] T. Timothy and J. Prestero, "Verification of a six-degree of freedom simulation model for the REMUS autonomous underwater vehicle," Thesis, Massachusetts Institute of Technology, Cambridge, MA, USA, 2001.

[21] T. I. Fossen, "How to incorporate wind, waves and ocean currents in the marine craft equations of motion," *IFAC Proceedings Volumes*, vol. 45, no. 27, pp. 126–131, 2012.

[22] X. Xiang, L. Lapierre, and B. Jouvencel, "Smooth transition of AUV motion control: from fully-actuated to under-actuated configuration," *Robotics and Autonomous Systems*, vol. 67, pp. 14–22, 2015.

[23] M. Breivik and T. I. Fossen, "Path following for marine surface vessels," in *Proceedings of the Oceans '04 MTS/IEEE Techno-Ocean '04 (IEEE Cat. No.04CH37600)*, pp. 2282–2289, Kobe, Japan, November2004.

[24] O. J. Sordalen and O. Egeland, "Exponential stabilization of nonholonomic chained systems," *IEEE Transactions on Automatic Control*, vol. 40, no. 1, pp. 35–49, 1995.

[25] F. Alonge, F. D'lppolito, and F. M. Raimondi, "Trajectory tracking of underactuated underwater vehicles," *in Proceedings of the the 40th IEEE Conference on decision and Control*, vol. 6, Orlando, FL, USA, December, 2001.

[26] H. K. Khalil, *Nonlinear Systems*, Prentice-Hall, Upper Saddle River, NJ, USA, 3rd edition, 2002.

[27] C. Dai, N. Zhang, and Z. Shen, "An adaptive nonlinear iterative sliding mode controller based on heuristic critic algorithm," in *Proceedings of the 2016 IEEE International Conference on Information and Automation (ICIA)*, pp. 419–424, Ningbo, China, August 2016.